JOURNAL OF MATERIALS SCIENCE: MATERIALS IN MEDICINE 12 (2001) 497–501

Nano-crystallization and surface analysis of electrolytic ZrO_2 coatings on Co-Cr alloy

S. K. YEN*, H. C. HSU
Institute of Materials Engineering, National Chung Hsing University, Taichung, Taiwan 40227
E-mail: skyen@dragon.nchu.edu.tw

Zirconia coatings were formed on Co-Cr substrates by electrolytic deposition. The microstructure of electrolytic zirconia-coated films on Co-Cr substrates was examined. According to the results of ESCA, the bonding energies of ZrO_2 coating surface layer which changed with the annealing temperature from 400 °C, 500 °C to 600 °C are attributed to amorphous (a), tetragonal (t) and monoclinic (m) structure, respectively. The X-ray diffraction (XRD) of the coatings on the Co-Cr substrates annealed at 400, 500 and 600 °C revealed the major crystallization from m through t and then to $m + t$. However, TEM observations clearly showed that the interface layer of the coatings were nanosize crystallites, first the formation of tetragonal and monoclinic ZrO_2 structures. These different phase transformations are mainly due to the different surface energy of ZrO_2 coating in air, in bulk or on Co-Cr alloy.

1. Introduction

Various methods of ceramic coatings have been considered to improve the wear and corrosion resistance of metallic implants. For example, physical vapor deposition (PVD) technique has been introduced in dental implant appliances as thin film technique, with ion-sputtering [1, 2] and ion-plating [3]. Further, porcelain has long been used to provide metal with an aesthetic and corrosion resistance covering.

Electrodeposition by controlling potential and using chemical aqueous solutions can obtain ceramic coatings over metal substrates [4, 5]. This method offers a number of advantages over other conventional coating methods (CVD, sputtering etc) including: low temperature process, low cost equipment, easy to control microstructure of coatings, and can be used in any shape of substrates [6]. These advantages make this method more attractive to metallic implants.

Cobalt-chromium alloys are used widely in dental implants, bridgework, and as base-plates in complete dentures. Their main use is as a framework in removable partial dentures. Several components of these alloys are cytotoxic [7, 8]. The dissolution properties of several components of these alloys in cell culture medium have also been reported [9]. The allergic and carcinogenic potential of cobalt, chromium and nickel is well documented [10, 11].

Zirconia is well known for its superior properties of mechanical strength and wear resistance [12, 13]. The preparation of ZrO_2 coatings on metallic substrates by sol-gel methods, using electrodeposition techniques can have a great influence on chemical durability. The process offers advantages for modifying properties of substrates by low temperature treatment. The sol-gel method has also been employed for fabricating ceramic coatings [14, 15]. These features are all of significance in fabricating advanced ceramics with improved properties. Various methods of obtaining ceramic coatings have been considered [16–18], and various theories have been advanced to explain why the two materials bond. One of the established bond-strength tests is the planar shear test [19]. Another commonly used test is the flexural test, which requires layers of porcelain to be bonded to a strip or plate of metal [20–22]. The coated metal plate is flexed in a controled manner until the porcelain fractures. Ceramic coatings have been and continue to be studied as a means of improving the *in vivo* performance of orthopedic and dental load-bearing implants [14, 15, 18].

In a previous study [23], cobalt-chromium alloys were used as the substrate and electrolytic ZrO_2 coatings was obtained from $ZrO(NO_3)_2$ aqueous solution at room temperature. This technique may improve the corrosion resistance and decrease the ion release. In this study, the phase transformation of ZrO_2 coated films on the Co-Cr substrates is further investigated by X-ray diffraction (XRD) and electron spectroscopy for chemical analysis (ESCA). In addition, the microstructure and grain size of the coated films are examined by using transmission electron microscopy (TEM).

*Author to whom all correspondence should be addressed.

2. Experimental procedure

2.1. Sample preparation

Dental cobalt-chromium alloy ingot (Remanium GM800, Dentaurum) was used as a substrate of electrolytic ZrO_2 coating. The chemical composition was Co (63.3 wt %), Cr (30 wt %), Mo (5 wt %), Si (1 wt %), C (0.3 wt %) and Mn (0.2 wt %). Cylinders of Co-Cr alloy were fabricated. Wax patterns (15 mm diameter, 16 mm length) were invested, then induction cast according to the manufacturer's recommendations. After devesting, the ingot was cut into discs with 15 mm diameter, 1 mm thickness. All disk specimens were finally polished to mirror-like by 0.5 μm Al_2O_3 powder. Each specimen was cleaned with acetone (organic debris removal), followed by a treatment for 5 min in an ultrasonic bath filled with deionized water, and then dried by N_2 air gun.

2.2 Electrolytic coating and differential scanning calorimetry (DSC) analysis

The disk alloy was used as the cathode, the graphite the anode, and the saturated calmel (SCE) the reference electrode in a 0.625 M $ZrO(NO_3)_2$ aqueous solution, pH = 2.46. The electrolytic deposition was conducted at a cathodic potential -1.5 V for 500 s using an EG&G M273A Potentiostat. Specimens with $Zr(OH)_4$ gel coating are then naturally dried and annealed at 400, 500 and 600 °C for 1 h in air. The thermal behavior of collected $Zr(OH)_4$ gel was analyzed by DSC (6200, SEIKO) with a heating rate of 15 °C/min from 25 °C to 600 °C.

2.3. ESCA

The annealed samples were characterized by electron spectroscopy for chemical analysis (ESCA) on a Fison (VG) ESCA 210. Each sample was analyzed by survey and high resolution spectra employing a Mg Kα X-ray anode, energy 1253.6 eV. From the survey spectra, the qualitative and quantative elemental composition and state of the uppermost layer were computed. The binding states of elements O and Zr were obtained by acquistition of high-resolution spectra and subsequent curve-fitting. The assignment of each curve-fit to a specific binding energy was characteristic of the compounds formed on the Co-Cr alloys.

2.4. XRD and TEM

The XRD analysis of the coatings on Co-Cr substrates was carried out with a MAC MO3X-HF Diffraction Japan diffractiometer, using CuK_α radiation at 40 kV and 30 mA (wavelength 1.5418 Å). The coatings were scanned from 20° to 100°, at a scan rate of 1°/min. The XRD spectra were identified using the Joint Committee of Powder Diffraction Standard (JCPDS) card. TEM was also analyzed using a Zeiss EM 902 microscopy at 80 kV.

3. Results and discussion

The Co-Cr alloys can be electrolytically coated with ZrO_2 at proper potential. It can be found that the surface of the Co-Cr alloy was almost coated completely and homogeneously [23], though there are few micro-cracks on the ZrO_2 coatings. These micro-cracks possibly occur because the evaporation rate of H_2O from the surface of the gel is higher than the diffusion rate of the H_2O from the bulk of the gel. Another possible reason for the cracks is the accommodating stress between the coating and substrate. The microcracks were also examined using TEM, as shown in Fig. 1. Fortunately, the TEM micrograph reveals that ZrO_2 still existed in the small cracks. Such that, the ZrO_2 coating can provide a good corrosion behavior for the Co-Cr alloy [23].

A strong endothermic peak at 91.5 °C on the DSC diagram is observed, as shown in Fig. 2. Mueller *et al.* [24] reported that there was a dynamic reaction complementary to isothermal reaction leading at 95 °C, which is almost consistent with the results here. The peak, at 91.5 °C can be attributed to the evaporation of the water contained in the materials. The heat of water evaporation in $Zr(OH)_4$ (658 J/g) is greater than in pure water (539 J/g) due to a stronger bonding in $Zr(OH)_4$. This argument has also been supported by the TGA (thermal gravimetric analysis) curve which showed 80% weight loss around this peak [25]. Fig. 2 also exhibits an exothermic peak at 478.4 °C for the $Zr(OH)_4$ gel. This peak may be attributed to the condensation followed by crystallization to a tetragonal structure, as shown in XRD diagrams for a collected $Zr(OH)_4$ gel [25].

On the other hand, ESCA diagrams, as shown in Fig. 3 reveal that the bonding energy peaks of O-ls in ZrO_2 coatings after being annealed at 400, 500 and 600 °C are 530 eV, 532.4 eV and 531.8 eV, respectively. The bottom one (400 °C) is lower and broadened on its left shoulder. The broadened peak means the bonding energy has a wider distribution and is more relaxed, possibly due to amorphous structure. The other two sharp peaks of 500 °C and 600 °C, respectively, indicate two more fixed bonding energies due to the crystallization of two

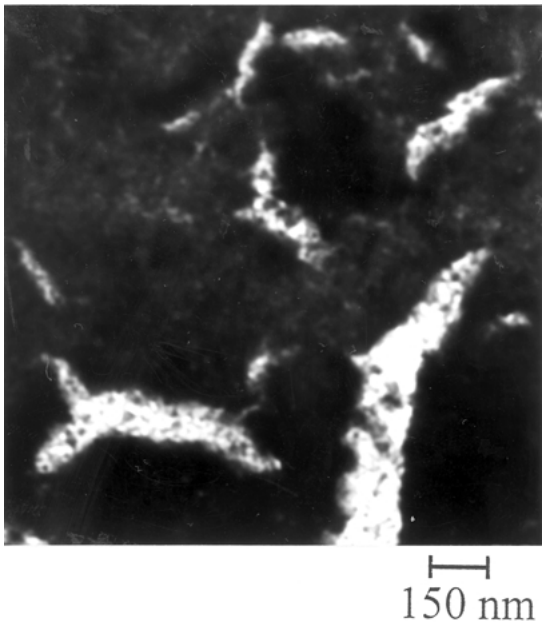

Figure 1 TEM micrograph of ZrO_2 coatings after annealing at 500 °C for 1 h, exhibits ZrO_2 films still on the micro-cracks.

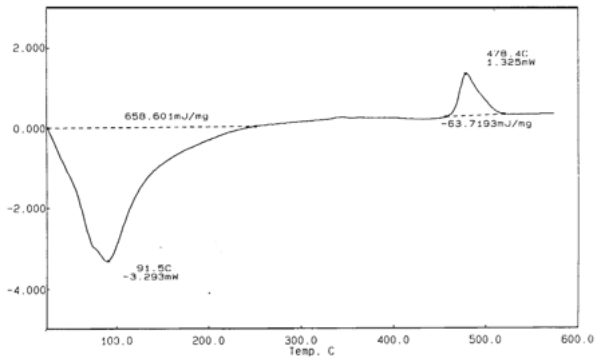

Figure 2 DSC analysis of $Zr(OH)_4$ gel in alumina crucible and static air, from 25 °C to 600 °C.

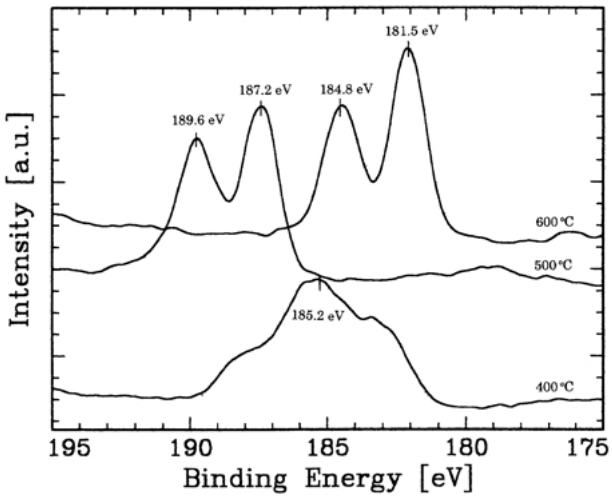

Figure 4 Zr-3d ESCA spectra of ZrO_2 coatings after annealing at 400, 500 and 600 °C for 1 h.

different structures. Furthermore, Fig. 4 shows the bonding energy peaks of Zr-3d ESCA spectra in ZrO_2 coatings after annealing at 400, 500 and 600 °C. The two main energy peaks are Zr-$3d_{3/2}$ and Zr-$3d_{5/2}$ of ZrO_2. The positions of the two peaks have changed with the different annealing temperature. For the same reason, the Zr-$3d_{3/2}$ and $3d_{5/2}$ and peaks broadened and then overlapped to form another peak at 185.2 eV for the specimen annealed at 400 °C. Two definite binding energy peaks of 187.2 eV and 189.6 eV were found after being annealed at 500 °C and the other two 181.5 eV and 184.8 eV were found after being annealed at 600 °C. Consequently, it is concluded that the surface layer structure of ZrO_2 coatings has changed with the annealing temperature and the chemical bonding shifts are mainly due to three different structures, possibly amorphous, tetragonal and monoclinc ZrO_2.

Fig. 5 shows the XRD diagrams of the Co-Cr alloy before and after electrolytic coating with ZrO_2, then annealing at 400, 500 and 600 °C, respectively. The XRD pattern of the Co-Cr alloy after electrolytic coating shows peaks corresponding to the Co-Cr alloy and ZrO_2 ceramic. After annealing at 400 °C, the monoclinic ($\bar{1}11$) preferred peak was detected, as shown in Fig. 5(b). Only the tetragonal (111) peak of ZrO_2 deposits was observed at 500 °C, as shown in Fig. 5(c). Then, the mixture of tetragonal and monoclinic phase was found at 600 °C, as shown in Fig. 5(d). This means that the 600 °C annealing induced the phase transformation from tetragonal to monoclinic again. Therefore, a full transformation to the monoclinic phase could be realized at higher temperatures (> 600 °C). Similar results have been found in the ZrO_2 coating on Ti-6Al-4V [23]. It has been concluded that monoclinic ($\bar{1}11$) preferred orientation formed at lower annealing temperature is due to the interface energy between ZrO_2 and metal substrate. Although results of XRD are different from those of ESCA which conclude three different structures on the surface layer at three different annealing temperatures, it is recognized that the surface layer structure may be different from the interface or the bulk. This is because the former is faced with air and the latter is faced with metal or itself. This argument is further supported by the phase transformation of ZrO_2 without metal substrate effect which is also faced with air and reveals a different transformation process from amorphous (400 °C) to tetragonal (500 °C) and the monoclinic (600 °C) [25]. Therefore, it is further suggested that the surface layer structures after annealing at 400 °C, 500 °C and 600 °C are amorphous, tetragonal and monoclinic, respectively. On the other hand, XRD diagrams show that the major phases (or the film bulk) are monoclinic, tetragonal and two mixed phases, respectively, as listed in Table I.

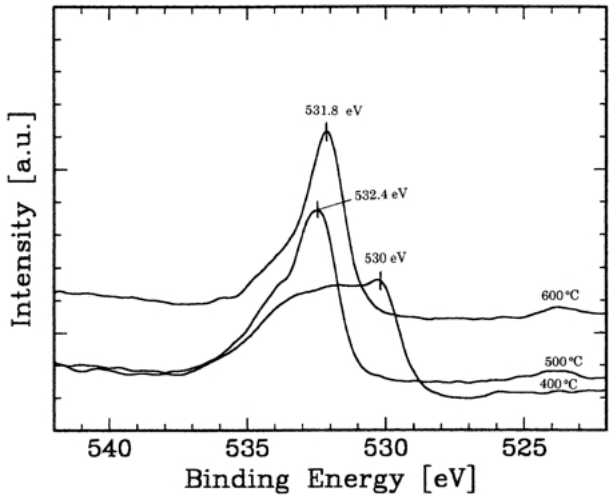

Figure 3 0-1s ESCA spectra of ZrO_2 coatings after annealing at 400, 500 and 600 °C for 1 h.

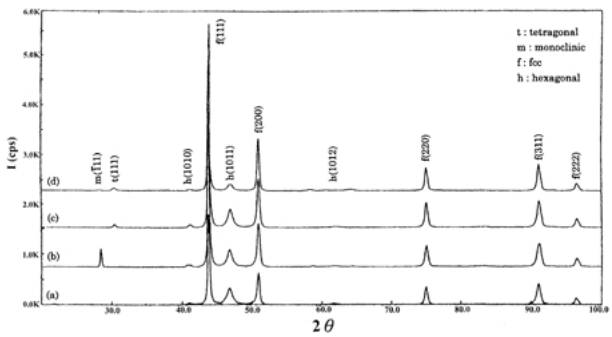

Figure 5 XRD patterns of the Co-Cr alloy (a) before coating, and after ZrO_2 coating and annealing at (b) 400 °C (c) 500 °C and (d) 600 °C for 1 h.

TABLE I Suggested surface layer structure of ZrO_2 on the Co-Cr alloy by ESCA and major phases by XRD

Annealing temperature	400 °C	500 °C	600 °C
Surface layer	Amorphous	Tetragonal	Monoclinic
Major phases	Monoclinic	Tetragonal	Monoclinic + Tetragonal

TABLE II Crystal structures of ZrO_2 interface layers on Co-Cr alloys, analyzed by TEM diffraction, as shown in Fig. 6(c) 400 °C, Fig. 7(c) 500 °C, and Fig. 8(c) 600 °C

Annealing temperature	400 °C	500 °C	600 °C
Planes of monoclinic phase	(100)	(100)	(011)
	(111)	(111)	(111)
	(002)	(002)	(021)
	(121)	(121)	(102)
	(122)	(122)	(022)
	(202)	(202)	(130)
	(131)	(131)	
Planes of tetragonal phase			(111)
			(112)
			(222)
Interface layer structure	Monoclinic	Monoclinic	Monoclinic + Tetragonal

To further study the structure of the ZrO_2 interface layer on Co-Cr alloys, TEM was conducted on specimen thickness 30 nm which was estimated by thickness fringe. Fig. 6 shows the TEM micrographs of the specimen after annealing at 400 °C for 1 h. The nanosize (< 3 nm) ZrO_2 crystalline grains are found in Fig. 6(a) (B.F., bright field) and Fig. 6(b) (D.F., dark field). The diffraction patterns as shown in Fig. 6(c) indicate a monoclinic structure which is the same as XRD. This means that monoclinic is also the major phase. The monoclinic structure without obvious grain growth was also found after annealing 500 °C as shown in Fig. 7(a–c). The corresponding planes to each ring are listed in Table II. However, this structure is different from that of XRD which showed a tetragonal structure. At 500 °C, the major structure is tetragonal but the interface layer structure was monoclinic due to different surface energy. Fig. 8 shows TEM micrographs of the specimen after annealing at 600 °C. The monoclinic phase was mixed with the tetragonal phase and obvious grain growth ($5 \sim 10$ nm) was found, as shown in Fig. 8(a–c). The interface ZrO_2 structure has also changed with annealing temperature, but in a different way due to the different surface energy on Co-Cr alloy.

4. Conclusion

An electrolytic deposition has been applied to produce coatings of zirconia on Co-Cr alloy. The microstructural evolution in ZrO_2 coated film on Co-Cr alloys associated with the amorphous (a), monoclinic (m), tetragonal (t) transition has been investigated. For 1 h annealing, nanosize grains were formed. Through ESCA, XRD and TEM analysis, the phase transformations of surface

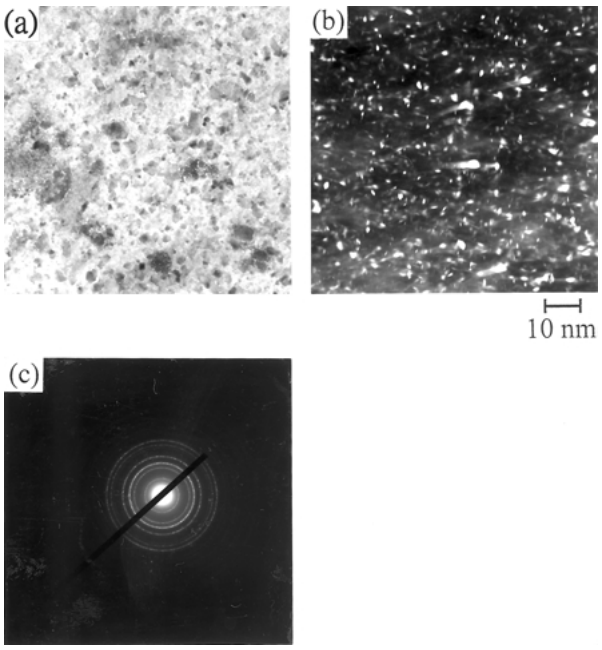

Figure 6 TEM micrographs (a) B.F., (b) D.F. and (c) diffraction pattern of ZrO_2 coatings on the interface, after annealing at 400 °C for 1 h.

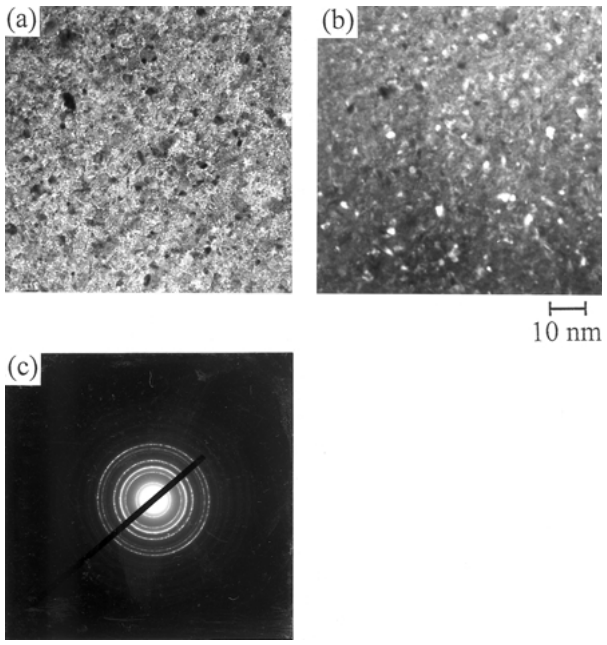

Figure 7 TEM micrographs (a) B.F., (b) D.F. and (c) diffraction pattern of ZrO_2 coatings on the interface, after annealing at 500 °C for 1 h.

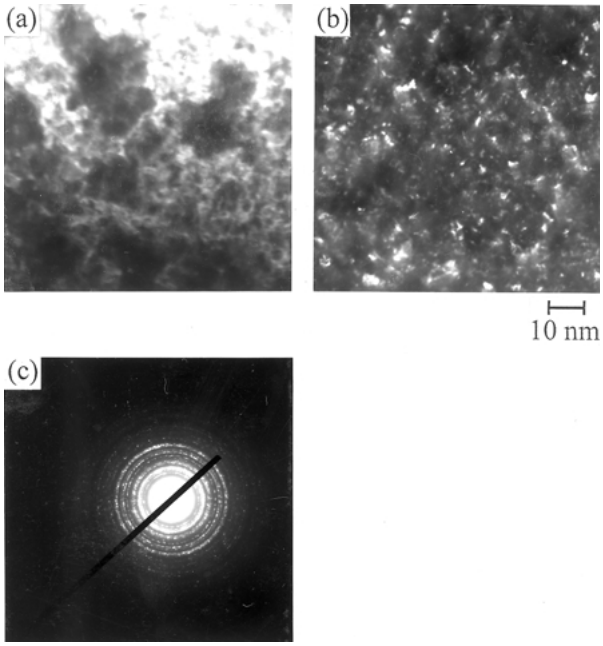

Figure 8 TEM micrographs (a) B.F., (b) D.F. and (c) diffraction pattern of ZrO_2 coatings on the interface, after annealing at 600 °C for 1 h.

layer, major phases (or the film bulk) and interface layer at 400 °C, 500 °C and 600 °C are $a \rightarrow t \rightarrow m$, $m \rightarrow t \rightarrow m + t$, and $m \rightarrow m \rightarrow m + t$, respectively. These different phase transformations are mainly due to the different surface energy of ZrO_2 in air, in bulk or on Co-Cr alloys.

Acknowledgments

The authors are grateful for the support of this research by the National Science Council Republic of China under Contract No. NSC 87–2213–E–005–022.

References

1. W. R. LACEFIELD, *J. Oral Implantol*. **20** (1994) 214.
2. D. R. COOLEY, A. F. van DALLAEN, J. O. BURGESS and A. S. WINDELER, *J. Prosthet. Dent*. **67** (1992) 93.
3. M. YOSHINARI, Y. OHTSUKA and T. DERAND, *Biomaterials* **15** (1994) 529.
4. L. GAL-OR, I. SILBERMAN and R. CHAIM, *J. Electrochem. Soc*. **138** (1991) 1939.
5. S. K. YEN and T. Y. HUANG, *Mat. Chem. Phy.* **56** (1998) 214.
6. K. IZUMI, M. MURAKAMI, T. DEGUCHI, A. MORITA, N. TOHGE and T. MINAMI, *J. Am. Ceram. Soc*. **72** (1989) 1465.
7. T. STENBERG, *Scand. J. Dent. Res.* **90** (1982) 472.
8. Z. L. SUN, J. C. WATAHA and C. T. HANKS, *J. Biomed. Mater. Res*. **34** (1997) 29.
9. J. C. WATAHA, R. G. CRAIG and C. T. HANKS, *J. Dent. Res.* **70** (1991) 1014.
10. R. W. PHILLIPS, ''Skinner's Science of Dental Materials'', 8th edn (Philadelphia, W. B. Saunders, 1982).
11. P. R. BOUCHARD, J. BLACK, B. A. ALBRECHT, R. E. KADERLY, J. O. GALANTE and B. U. PAULI, *J. Biomed. Mater. Res*. **32** (1996) 37.
12. G. WILLANN, H. J. FRUH and H. G. PFAFF, *Biomaterials*, **22** (1996) 2157.
13. I. THOMPSON and R. D. RAWLINGS, *Biomaterials* **11** (1990) 505.
14. M. J. FILIAGGI, R. M. PILLIAR and D. ABDULLA, *J. Biomed. Mater. Res*. **33** (1996) 239.
15. M. J. FILIAGGI, R. M. PILLIAR, R. YAKUBOVICH and G. SHAPIRO, *ibid.* **33** (1996) 225.
16. J. RIEU, *Clin. Mater*. **12** (1993) 227.
17. M. SHIRKHANZADEH, *J. Mater. Sci.: Mater. Med.* **3** (1992) 322.
18. M. YOSHINARI, Y. WATANABE, Y. OHTSUKA, and T. DERAND, *J. Dent. Res.* **8** (1997) 1485.
19. D. H. ANTHONY, A. P. BURNETT, D. L. SMITH and M. S. BROOKS, *ibid.* **49** (1970) 27.
20. K. J. ANUSAVICE, R. D. RINGLE and C. W. FAIRHURST, *J. Biomed. Mater. Res.* **11** (1977) 701.
21. K. J. ANUSAVICE, P. H. DEHOFF and C. W. FAIRHURST, *J. Dent. Res*. **59** (1980) 608.
22. I. A. HAMMAD, R. J. GOODKIND and W. W. GERBERICH, *J. Prosthet. Dent*. **58** (1987) 431.
23. H. C. HSU and S. K. YEN, *Dent. Mater*. **14** (1998) 339.
24. H. J. MUELLER, M. S. BAPNA and P. L. FAN, *J. Oral. Rehab.* **21** (1994) 699.
25. S. K. YEN, *J. Electrochem. Soc*. **146** (1999) 1392.

Received 3 November 1999
and accepted 26 January 2000